DOI: https://10.83080/rejost.vol6no10.365

Researchers Journal of Science and Technology (REJOST)

Design and Implementation of a Microcontroller-Based Automatic Phase Selector Using Dual-Timescale Voltage Stability Evaluation

Omoroghomwan E. A., Okoyenhan M., Odhegba O. J., Idialu E. E., Ehigiele E. O., Opadeji O. F.

Abstract

Automatic phase selectors that rely on instantaneous voltage readings are prone to unnecessary switching during transient disturbances, accelerating contactor wear. This paper presents a microcontroller-based automatic phase selector that evaluates voltage-to-time stability using two independent timescales. A four-band voltage classification is implemented: a voltage strictly below 170 V or strictly above 250 V triggers an immediate fault with no tolerance; a grace zone ($170 \leq V < 180$ V and $240 < V \leq 250$ V) is tolerated for up to five seconds before being treated as a fault; an acceptable band ($180 \leq V \leq 240$ V) is never treated as a fault; and a recovery band (200–235 V) that a phase must hold continuously for one hour before earning full automatic trust. The system uses an ESP32, four PZEM-004T sensing modules, three 100 A contactors with dual-layer interlocking, and a 2.8-inch thin-film transistor (TFT) display. Bench testing yielded a switching response time of 1.93 seconds, voltage sensing accuracy with a maximum absolute error of ±0.50%, and current sensing accuracy with a maximum absolute error of ±0.50% at the 2–12 A test points the bench could supply. High-current protection was verified by injecting simulated current values because the bench could not supply 80–98 A. The prototype demonstrates the feasibility of time-based phase selection, but further testing with calibrated instruments, representative loads, and a physical high-current test setup is needed before field deployment or claims of improved contactor lifespan can be established.

✉ Omoroghomwan E. A.: efosa.omoroghomwan@uniben.edu

Department Of Electrical/Electronic Engineering, Faculty of Engineering, University of Benin, Benin City, Edo State, Nigeria

Keywords: Automatic phase selector; voltage stability; time-based evaluation; ESP32; PZEM-004T; dual-timescale algorithm; residential power supply

Article history

Received: September 5, 2026
Received in revised form: October 29, 2026
Accepted for publication: November 2, 2026
Available online: November 20, 2026

Table of Nomenclature

SYMBOL	DESCRIPTION	UNIT
V_hard_min	Hard minimum voltage limit (170 V)	V
V_hard_max	Hard maximum voltage limit (250 V)	V
V_accept_min	Acceptable band minimum (180 V)	V

V_accept_max	Acceptable band maximum (240 V)	V
V_recover_min	Recovery band minimum (200 V)	V
V_recover_max	Recovery band maximum (235 V)	V
GRACE_MS	Grace period duration (5000 ms)	ms
STABILIZE_TIME_MS	Recovery window duration (3,600,000 ms)	ms
PHASE_SAMPLE_TIMEOUT_MS	Maximum allowable sample age (1200 ms)	ms
CONTACTOR_DEAD_TIME_MS	Dead-time between relay switching (1000 ms)	ms
faulted[i]	Boolean fault flag for phase i	—
isStable[i]	Boolean trust flag for phase i	—
acceptableExitTime[i]	Timestamp when phase i left acceptable band	ms
healthyStartTime[i]	Timestamp when phase i entered recovery band	ms
lastSampleTime[i]	Timestamp of last valid sample for phase i	ms
I_B	Maximum expected continuous load current	A
P_total	Total connected real power	W
V	Nominal supply voltage (230 V)	V
cos θ	Power factor (0.85 assumed)	—
I_contactor	Required contactor current rating	A
S	Conductor cross-sectional area	mm^2
k	Material/insulation constant (115 for PVC copper)	—
I^2t	Let-through energy	A^2s
$U_{N'N}$	Neutral displacement voltage	V
Y_i	Load admittance on phase i	S
R1	Level-shifter HV-side pull-up resistor (10 kΩ)	Ω
R2	Fail-safe pull-down resistor (1 kΩ)	Ω
C	Snubber capacitor (0.1 µF)	F
f	Supply frequency (50 Hz)	Hz
Xc	Capacitive reactance	Ω
I_{leak}	Snubber leakage current	A
Iz	Effective cable current-carrying capacity	A
In	Miniature circuit breaker (MCB) nominal rating (63 A)	A
I_{cn}	MCB rated short-circuit breaking capacity (6000 A)	A
ΔV	Voltage drop	V
U_{L1}, U_{L2}, U_{L3}	Phase (line-to-neutral) voltages	V
Zi	Load impedance on phase i	Ω
V_{NodeA}	Relay-input node voltage with ESP32 output floating (Eq. 2)	V
P	Snubber resistor power dissipation (upper-bound estimate, Eq. 3)	W

1.0 Introduction

A reliable electricity supply is essential for economic productivity and industrial development. In developing countries such as Nigeria, however, the gap between electricity demand and dependable supply remains wide. Power failure or outage has been a major challenge to national development, as economic activities are at most times brought to a standstill (Ezirim et al., 2015). There are power-dependent processes that cannot be interrupted without serious consequences such as surgical operations in hospitals, inter-bank fund transfers, industrial production lines, and telecommunications infrastructure (Ezirim et al., 2015). As industrial processes and IT applications diversify, power consumers have adopted alternative means of supply like generators, inverters, and solar systems, to

compensate for the unreliability of electricity supplied by distribution companies (Ezirim et al., 2015; Adamu et al., 2025).

The introduction of changeover switches offered a means to transfer between the national grid and a generator, but this was originally done only through manual operations. Manual changeover systems have several limitations: the stress of physically turning the metal gear to effect the changeover, the inability to detect the level and sequence of the three phases, and the inability to select between phases for single-phase consumers (Ezirim et al., 2015).

At the distribution level, most residential and small commercial consumers are connected to only one phase of the three-phase supply, so power interruptions occur whenever the connected phase experiences a fault, voltage instability, or a total outage, even when the other two phases remain available. It is common in many residential areas for electricity to be present on one or two phases while another remains faulty, and most consumers are either unaware that an alternative phase is available or lack the technical expertise to switch phases safely. In the past, phase failure often disrupted operations in industries, offices, and homes, leading to situations where some appliances are mistakenly left on (Adamu et al., 2025). Frequent phase failures also led to manual switching of phases, causing delays, potential damages, and costly human errors (Uchechukwu, 2015). Manual phase switching carries real risk of electric shock, insulation breakdown, equipment damage, and fire (Uchechukwu, 2015; Adamu et al., 2025).

Unreliable supply carries economic cost for small businesses. Barbershops, welding shops, and food vendors that rely on petrol or diesel generators face daily fuel costs estimated between ₦500 and ₦5,000, depending on business size and consumption (Adeniyi, 2022), which erodes profitability and limits growth. Independent reports have documented the severity of supply interruptions in Benin City and other parts of Edo State (Sahara Reporters, 2023; Vanguard, 2023). Earlier work on the causes of erratic supply in Benin City is provided by Odior and Omadudu (2013).

In response to these challenges, the automatic phase selector was developed to detect available live phases and connect the electrical load to an active one automatically (Adamu et al., 2025). Some previous designs focused on detecting a single active phase and utilized electromechanical switches driven by transistors to connect the load to the live phase. When two or more phases are available, the circuit selects the most stable or suitable one for connection (Adamu et al., 2025).

However, automatic phase selectors documented in the literature carry structural weaknesses of their own. Most conventional selectors rely on a single instantaneous voltage reading, which triggers frequent phase transfers in response to transient sags or spikes rather than genuine, sustained outages. This constant switching accelerates mechanical contact wear, increases contactor arcing, and reduces the system's overall reliability. Comparator-based designs such as those of Asiwe and Usiaade (2021), Ish (2024), Oduobuk et al. (2014), and Ofualagba and Udoha (2017) compare the three phases continuously against each other and switch to whichever phase is healthy at that instant, but they have no way to distinguish a momentarily high reading from a genuinely stable phase. On the other hand, the threshold-based microcontroller designs such as those of Singh et al. (2017), Mbaocha (2012), Madueme et al. (2018), Akpan et al. (2019), Akinola et al. (2024), and Adesina et al. (2024) implemented the selection in microcontroller logic (live/dead checks, user-preset thresholds or threshold crossing) instead of analog comparators, but the switching decision was still made against a single reading rather than a sustained period of observation. A literature matrix comparing existing designs is provided in Table 1.

Table 1: Literature Matrix of Existing Phase Selector Designs

Author(S)	Controller Type	Sensing Method	Switching Criterion	Delay/Hysteresis	Load Monitoring	Interlocking	Experimental Validation
Asiwe & Usiaade (2021)	OP-AMP Comparators	Instantaneous Voltage	Comparator-based	None	No	No	Bench test
Ish (2024)	OP-AMP + Timer	Instantaneous Voltage	Comparator-based	Timer	No	No	Bench test
Oduobuk et al. (2014)	LM324 Comparators	Instantaneous Voltage	Highest voltage	None	No	No	Simulation
Ofualagba & Udoha (2017)	Comparator circuits	Instantaneous Voltage	Comparator-based	None	No	No	Simulation
Singh et al. (2017)	ARM7	Live/Dead Check	Binary Logic	None	No	No	Bench test
Mbaocha (2012)	AT89C52	Live/Dead Check	Binary Logic	None	No	No	Bench test
Madueme et al. (2018)	PIC16F877A	Instantaneous Voltage	Highest instantaneous value	None	No	No	Bench test
Akpan et al. (2019)	Arduino Nano	Threshold-based	User-preset threshold	None	No	No	Bench test
Adesina et al. (2024)	ATMega328PU	Threshold-based	Threshold crossing	None	No	No	Bench test
Akinola et al. (2024)	PIC16F877A	Threshold-based	Threshold crossing	None	No	Not described	Simulation
Ezirim et al. (2015)	Relays/Contactors	Voltage sensing	Priority order	None	No	Electrical	Simulation
Adamu et al. (2025)	LM741 Comparators	Instantaneous Voltage	Highest voltage	None	No	No	Bench test
Proposed System	ESP32	Time-based (5s + 1hr)	Dual-timescale	5s grace, 1hr trust	Yes (PZEM-004T)	Hardware + Firmware	Bench test

In addition, most existing designs monitor grid-side parameters exclusively and ignore load-side current. When a connected load draws current approaching or exceeding the contactor's rated breaking capacity, the switching apparatus operates blind to that condition, risking contactor welding, thermal runaway, and fire. Recent research on automatic transfer switches has documented catastrophic failures arising from such design deficiencies, including neutral conductor loss leading to overvoltages approaching 400 V and the destruction of connected electronic equipment (Buică et al., 2026).

This paper presents a microcontroller-based automatic phase selector that addresses these gaps through dual-timescale voltage stability evaluation, load-side monitoring, and dual-layer electrical interlocking. The specific contributions of this work are:

1. A four-band voltage classification logic with a 5-second grace period for fault detection and a 1-hour recovery window for long-term trust.
2. Integrated load-side monitoring using a fourth PZEM-004T module to detect overload conditions and power factor deviations.
3. Dual-layer electrical interlocking implemented in both hardware (auxiliary contacts) and firmware (state machine and relay-driving code).
4. A fail-safe design with a 1 kΩ pull-down resistor at each relay input to ensure de-energization on microcontroller unit (MCU) failure.

The design aligns with emerging trends in low-cost, ESP32-based monitoring and protection systems (Cárdenas Magaña et al., 2026; Hidayat & Al-Faris, 2025; Mustofa, 2026; Sukadana et al., 2026).

1.1 Mathematical and Theoretical Background

The main contribution is a voltage-stability algorithm that evaluates phase conditions over two timescales. Rather than relying on a single instantaneous voltage reading, the algorithm continuously classifies each phase into one of four operating bands and applies two separate timing criteria, which is a short grace period for fault detection and a long recovery window for establishing trust. This section explains the logic governing each decision, while the corresponding implementation is provided as pseudocode in Algorithms 1–4 in Section 2.3.1.

1.1.1 Four-Band Voltage Classification

The firmware evaluates phase health using four voltage bands, illustrated in Figure 1. A voltage strictly below 170 V or strictly above 250 V is treated as an immediate fault, with no tolerance or delay; these are the absolute operating limits of the system. Within this envelope, the acceptable band ($180 \leq V \leq 240$ V) is never itself treated as a fault, and a phase operating in this range is considered healthy for load supply. Between the hard limits and the acceptable band sit two grace zones: $170 \leq V < 180$ V on the lower side and $240 < V \leq 250$ V on the upper side. A phase already supplying the load is permitted to remain in a grace zone for up to five seconds before the excursion counts against it as a fault. Finally, a narrower recovery band (200–235 V) governs whether an inactive phase is trusted as a new automatic target; a phase must hold continuously inside this band for one hour before earning full trust, and a single out-of-band sample resets the timer to zero.

1.1.2 Fault Decision Logic

The fault decision for each phase combines four checks, evaluated in order. First, if no valid sample has been received within the last 1.2 seconds (the sample timeout), the phase is treated as faulted, since the system cannot confirm its condition. Second, if the most recent sample is marked invalid by the sensor-read debounce logic, the phase is faulted. Third, if the voltage lies outside the hard limits of 170 V and 250 V, the phase is faulted immediately, with no grace period. Fourth, if the voltage lies within the acceptable band (180–240 V), the phase is

not faulted, and any accumulated grace timer is cleared. If the voltage lies in a grace zone ($170 \leq V < 180$ V or $240 < V \leq 250$ V), the phase is faulted only if it has remained outside the acceptable band for at least 5 seconds; otherwise, it is tolerated as a transient excursion.

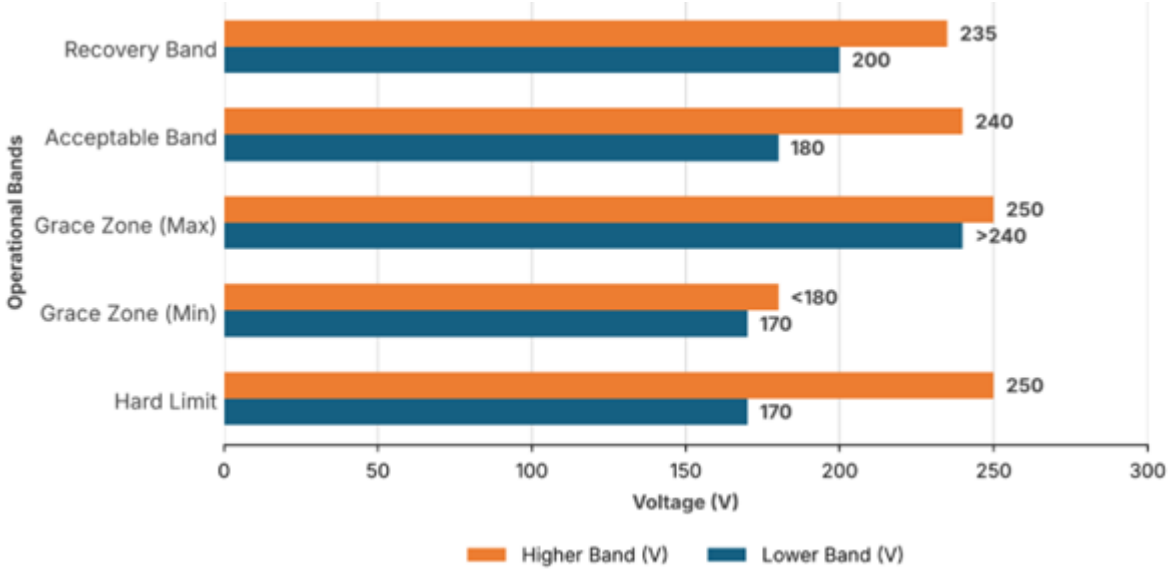


Figure 1: System operational band limits (grace zones: $170 \leq V < 180$ and $240 < V \leq 250$)

The grace timer is cleared whenever a sample is stale, invalid or outside the hard limits, as well as whenever the voltage returns to the acceptable band, so a grace → hard → grace sequence always starts a new 5-second count (Algorithm 1).

This combined logic ensures that brief voltage dips or spikes (such as those caused by motor starting or nearby load switching) do not trigger a phase transfer, while sustained excursions beyond the acceptable band are acted upon within a few seconds. A stale or missing sample is treated with the same severity as an out-of-band voltage, preventing the system from acting on outdated information.

1.1.3 Long-Term Trust Evaluation

Separate from the fault decision, the algorithm maintains a trust flag for each phase that determines whether it is eligible to become a new automatic target. A phase earns trust only after it has remained continuously within the recovery band (200–235 V) for one full hour. If at any point the phase leaves this band or if its sample becomes invalid or stale, the trust timer resets to zero, and the phase must begin the one-hour observation period afresh. This strict, no-partial-credit reset behavior ensures that a phase which is "mostly stable" but exhibits occasional excursions never accumulates enough uninterrupted good time to be trusted. The one-hour window is deliberately much longer than the 5-second grace period, operating at the timescale of grid recovery and regulation settling rather than transient disturbance.

1.1.4 Relation of the Timers to IEEE 1159 Power-Quality Categories

The 5-second grace period lies inside the temporary category of IEEE Std 1159-2019 (more than 3 seconds, up to 1 minute). An excursion that clears in under 3 seconds is an instantaneous or momentary event, and one that clears between 3 and 5 seconds is a temporary event that the grace timer still tolerates, so the grace period ignores all instantaneous and momentary events and the first 2 seconds of the temporary category. The 1-hour recovery window operates on a much longer timescale: the standard treats variations lasting more than 1 minute as long-duration RMS variations, but it sets no minimum or recommended time for showing that a supply is stable. Both timers are therefore the authors' own design choices, informed by these categories; IEEE Std 1159-2019 does not prescribe a grace period, recovery

time or trust window. The correspondence is by duration only. The voltage thresholds used here were set by the authors for a 230 V nominal supply and are not the per-unit magnitude ranges that the standard uses to define sags and swells, and the PZEM-004T modules report at about 1 Hz and are not power-quality monitors, so the firmware cannot resolve instantaneous or momentary events. The categories are used to give the timers a recognized vocabulary, not to claim compliance with the standard.

1.1.5 Neutral Displacement and Overvoltage Risk

A critical safety consideration in three-phase systems is neutral conductor integrity. Recent research has documented catastrophic failures arising from neutral loss in automatic transfer switches, where single-phase loads experience line-to-line voltages approaching 400 V (Buică et al., 2026). The neutral displacement voltage is given by Equation 1 (Buică et al., 2026, Eq. 1):

$$U_{N'N} = \frac{U_{L1}Y_1 + U_{L2}Y_2 + U_{L3}Y_3}{Y_1 + Y_2 + Y_3} \quad (1)$$

where $Y_i = 1/Z_i$are the load admittances. Phases with low-impedance loads experience undervoltage, while phases with high-impedance loads experience overvoltages approaching the line-to-line voltage (~400 V). This failure mode motivated the non-switching neutral design adopted in the proposed architecture, where the neutral conductor passes through solid metallic links rather than switchable contacts (Buică et al., 2026).

1.1.6 Contactor Endurance

The 100 A-class contactor specified in this project is the S9511M7. The published endurance data for the TeSys D 95 A class is used here as the closest available reference, since the S9511M7 datasheet does not provide equivalent endurance figures. The TeSys D 95 A contactor has a mechanical durability of 4 million cycles and an electrical durability of 1.2 million load-breaking cycles at 95 A under AC-3 duty (the IEC 60947-4-1 utilization category for starting squirrel-cage motors and switching them off while running). These ratings are defined under the manufacturer's stated test conditions (duty category, rated current and ambient temperature), and the maximum operating rate is a separate rating from the durability figures.

The 600 cycles/hour ceiling is derived from the 5-second grace period plus the 1-second dead time, assuming a worst-case scenario where a phase continuously oscillates in and out of the grace zone. This is a structural bound set by the firmware timing, not a direct comparison with the manufacturer's 3,600 cycles/hour operating rate, which is defined under different rating conditions.

At 600 cycles/hour sustained, the 1.2-million-cycle electrical rating would be reached in approximately 2,000 hours (about 83 days). However, the rapid-switching lockout and the 1-hour trust rule described in Section 2.3 are intended to keep the actual switching count well below this ceiling in practice; this is indicative only, because contactor endurance was not tested.

At a theoretical sustained transfer rate of one transfer per hour (8,760 transfers/year), the 1.2-million-cycle electrical rating would take approximately 137 years to exhaust. This figure is a theoretical cycle-count extrapolation only; it assumes a fixed transfer rate and does not account for contact aging, environmental conditions, the actual load category, fault interruptions, or the manufacturer's stated service conditions, and is not a prediction of service life. Table 2 summarizes this bound.

2.0 Materials and methods

2.1 Systems Architecture

The system has four functional blocks: sensing, control, switching/interlock, and user interface. Figure 2 shows the system block diagram. Each input phase is sensed by a PZEM-004T tapped at its MCB output, ahead of the contactor. A fourth

PZEM-004T monitors load-side current and power factor after the residual-current circuit breaker (RCCB). All four communicate with the ESP32 over a shared transmit line with separate receive pins, using the Modbus remote terminal unit (Modbus RTU) protocol. This architecture aligns with recent low-cost monitoring systems that demonstrate the PZEM-004T's suitability for residential applications, with reported mean absolute errors of 0.31 V for voltage and 0.008 A for current (Cárdenas Magaña et al., 2026).

Table 2: Contactor Switching-Frequency Bound vs. Manufacturer Endurance Rating

Parameter	Value
Contactor electrical durability (AC-3, 95 A)	1.2 million cycles (TeSys D 95 A reference)
Contactor max. rated operating rate	3,600 cycles/hour
Structural switching-rate ceiling	600 cycles/hour (control-logic bound)
Theoretical time to exhaust rating at 600 cycles/hour	~83 days
Assumed sustained transfer rate (theoretical)	1 transfer/hour
Implied time to exhaust electrical rating	~137 years (theoretical extrapolation only)

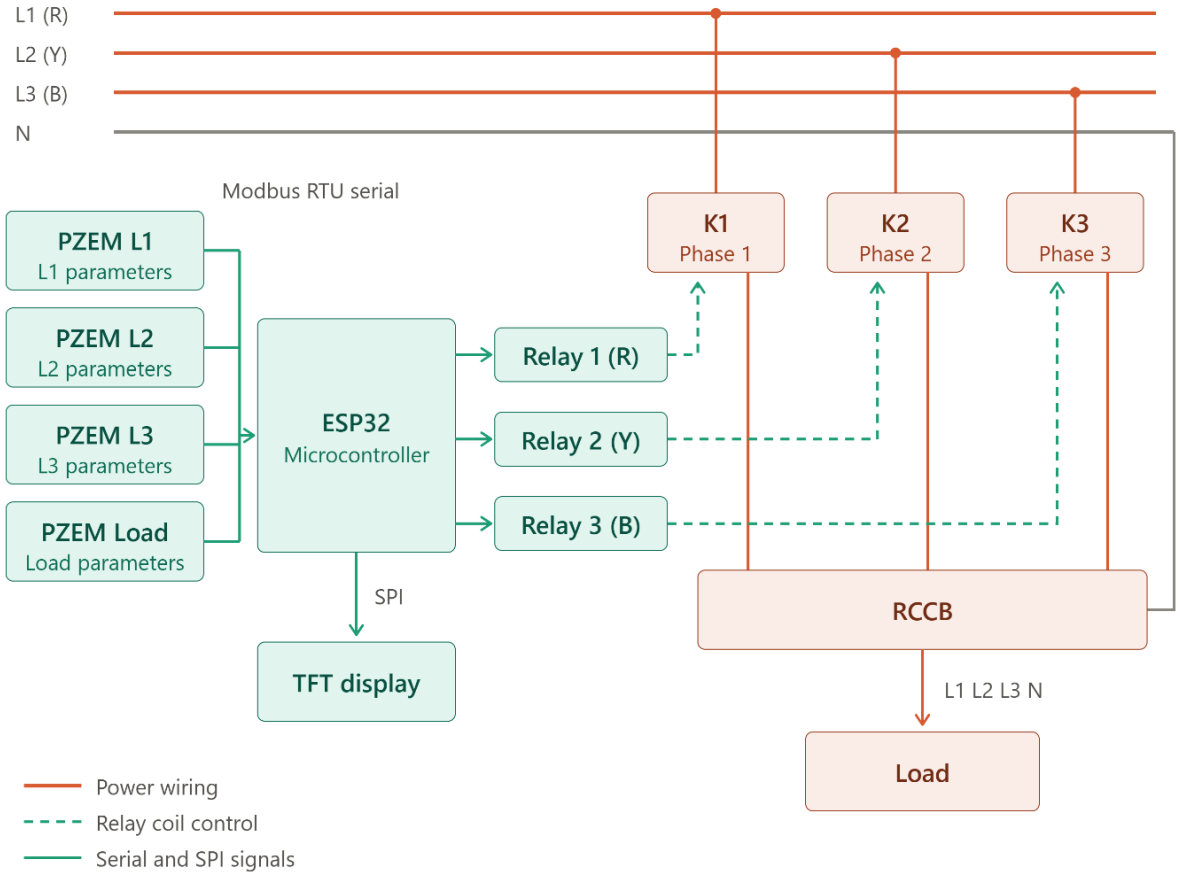


Figure 2: System Block Diagram

2.2 Hardware Design

2.2.1 Mechanical, Protection, and Interlocking Unit

Each phase passes through its own two-pole MCB, with a PZEM-004T tapped at the output. Three contactors handle phase switching, with outputs looped to a common node that passes through a single two-pole RCCB before the load. The switching control circuit establishes a strictly interlocked, MCU-controlled series path to safely manage phase selection. The actuation

sequence initiates with a 3.3 V logic HIGH signal from the ESP32 GPIO, which is stepped up to 5 V via a BSS138 bidirectional level shifter to trigger the active-HIGH 5 V relay module. A 1 kΩ pull-down resistor (R2) on the logic line forms a voltage divider with the level shifter's 10 kΩ pull-up (R1), ensuring fail-safe de-energization if the MCU output floats during reboot or power loss. Once the 5 V relay's normally open (NO) contacts close, they complete the 230 V AC neutral control feed. Crucially, this control feed reaches the selected S9511M7 contactor's A2 terminal only after passing through the hardwired emergency stop and the normally closed (NC) auxiliary contacts of the other two inactive contactors, while the A1 terminal remains directly tied to its respective phase live. Figure 3 shows the complete unit.

The critical importance of neutral conductor integrity in such systems is underscored by recent research documenting a real-world overvoltage incident caused by neutral loss in an automatic transfer switch (ATS), resulting in phase voltages of 54.2 V, 372.8 V, and 353 V (Buică et al., 2026). The proposed design avoids this failure mode by routing the neutral through solid metallic links rather than switchable contacts.

2.2.2 Power Supply

The control unit uses an isolated low-voltage supply. Table 3 summarizes the voltage rails.

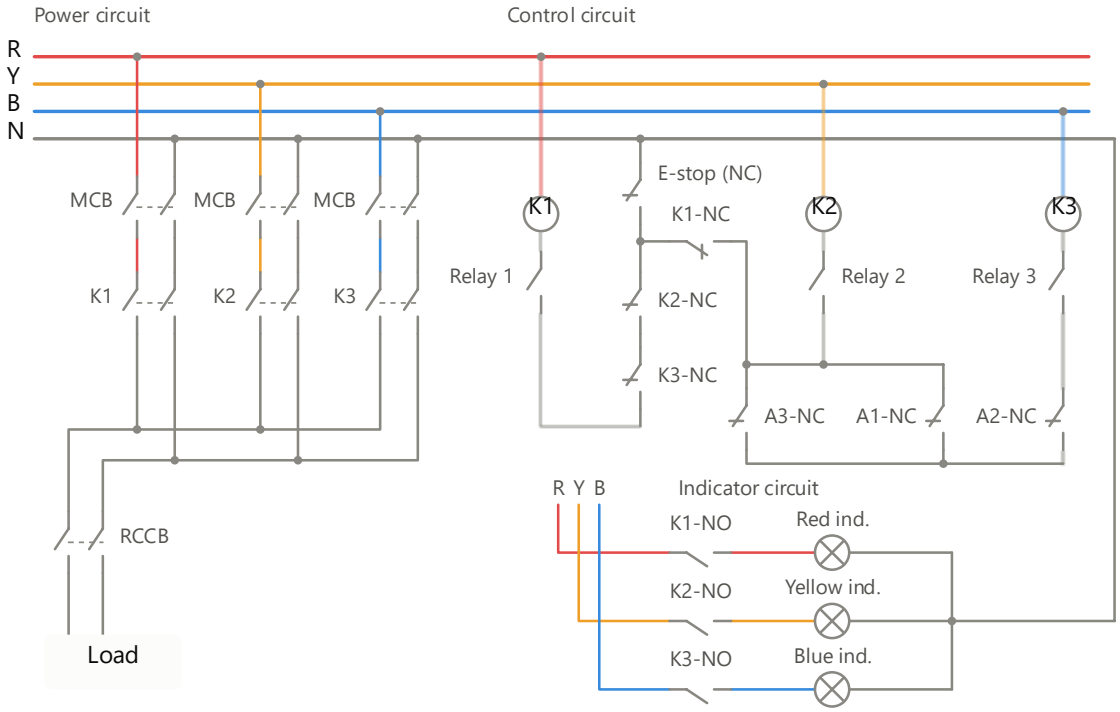


Figure 3: Mechanical, Protection and Interlocking Unit

Table 3: Control Voltage Rails and Their Loads

Rail	Voltage	Load	Typical Current
$V5_{RAW}$	5 V DC	PZEM-004T logic (×4), relay inputs, TFT backlight	~250 mA
V3.3	3.3 V DC	ESP32, TFT logic	~150 mA

A diode-OR arrangement lets the higher-voltage source supply the load. The battery pack charges through a dedicated single-cell charge circuit while mains is present and supplies the 5 V rail through the LX-2BUPS unit when mains is absent. This design follows established practices in low-cost IoT monitoring systems (Hidayat & Al-Faris, 2025; Mustofa, 2026).

2.2.3 Logic-Shifter Fail-Safe Design

Because the ESP32 operates at 3.3 V logic and the relay modules at 5 V, a bidirectional logic-level shifter sits between them. The shifter's 10 kΩ pull-up can float the relay input toward 5 V when the ESP32 is not driving it, energizing a contactor without MCU supervision. The ESP32 GPIO logic level is 3.3 V (Espressif Systems, 2022). A 1 kΩ pull-down resistor (R2) forms a voltage divider with the 10 kΩ pull-up (R1), giving Equation 2:

$$V_{NodeA} = 5V \times \frac{R2}{R1 + R2} = 5V \times \frac{1k\Omega}{10k\Omega + 1k\Omega} = 0.45V \quad (2)$$

This is well below the logic-HIGH threshold, keeping the contactor de-energized when the ESP32 floats. Figure 4 shows this circuit.

2.2.4 Coil Snubber Protection

Each contactor coil has an RC snubber (100 Ω, 1 W resistor + 0.1 µF capacitor) in parallel with a 10D471 metal-oxide varistor (MOV) rated at 470 V. A conservative upper-bound estimate of the resistor power dissipation, based on the capacitor energy circulating through the resistor each half-cycle, is given by Equation 3:

$$P = \frac{1}{2}CV^2f = \frac{1}{2} \times 0.1\mu F \times 230^2 \times 50 \approx 0.13W \quad (3)$$

A 1 W resistor gives an eightfold margin. The leakage current through the snubber is given by Equations 4 and 5:

$$X_c = \frac{1}{2\pi fC} \approx 31.8k\Omega \quad (4)$$

$$I_{leak} \approx \frac{230V}{31.8k\Omega + 100\Omega} \approx 7.2mA \quad (5)$$

This is too small to hold a coil energized but was accounted for in the interlock design.

2.3 Software Design

2.3.1 Firmware Structure

The main loop performs four tasks: reading PZEM-004T sensors, evaluating phase stability, advancing the switching state machine, and refreshing the display and dashboard. Complete pseudocode for the core algorithms is provided in Algorithms 1–4 below.

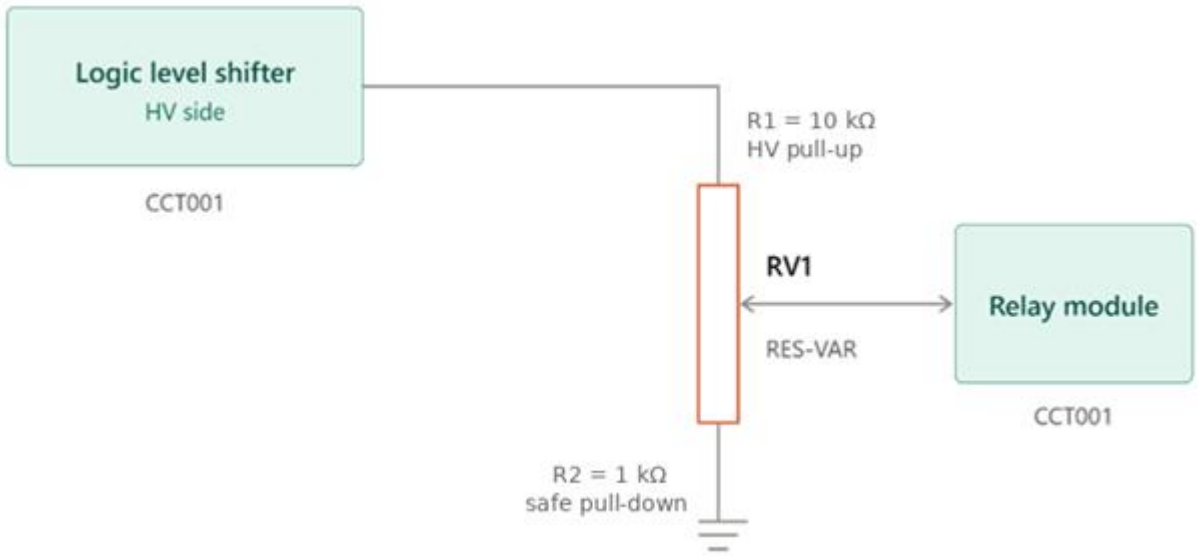


Figure 4: Logic Level Shifter and Fail-Safe Pull-Down

Algorithm 1: Voltage Stability Evaluation (run once per phase, per loop pass)

```
for each mains phase i in {1, 2, 3}:
  if lastSampleTime[i] == 0 or (now() - lastSampleTime[i]) > PHASE_SAMPLE_TIMEOUT_MS:
    faulted[i] = TRUE
    acceptableExitTime[i] = 0
  else if not valid[i]:
```

```
    faulted[i] = TRUE
    acceptableExitTime[i] = 0
  else if voltage[i] < V_HARD_MIN or voltage[i] > V_HARD_MAX:
    faulted[i] = TRUE
    acceptableExitTime[i] = 0
  else if V_ACCEPT_MIN <= voltage[i] <= V_ACCEPT_MAX:
    faulted[i] = FALSE
    acceptableExitTime[i] = 0
  else:
    if acceptableExitTime[i] == 0:
      acceptableExitTime[i] = now()
      faulted[i] = FALSE
    else:
      faulted[i] = (now() - acceptableExitTime[i]) >= GRACE_MS

  if valid[i] and (now() - lastSampleTime[i]) <= PHASE_SAMPLE_TIMEOUT_MS
    and V_RECOVER_MIN <= voltage[i] <= V_RECOVER_MAX:
    if healthyStartTime[i] == 0:
      healthyStartTime[i] = now()
    if now() - healthyStartTime[i] >= STABILIZE_TIME_MS:
      isStable[i] = TRUE
  else:
    healthyStartTime[i] = 0
    isStable[i] = FALSE
```

Algorithm 2: Switching Decision Function and State Machine Tick

```
function chooseTargetRelay():
  if currentControlMode == MODE_AUTO:
    if millis() < BOOT_OBSERVE_MS:
      return 0
    for phase in [1, 2, 3]:
      if phaseIsSafe(phase):
        return phase
    if currentActiveRelay > 0 and not activePhaseHasFault(currentActiveRelay):
      return currentActiveRelay
    return choose Best Acceptable Phase()
  else:
    if manualRequestIsFresh(manualTargetRelay) and phaseAcceptableGeneral(manualTargetRelay):
      return manualTargetRelay
    if currentActiveRelay > 0 and not activePhaseHasFault(currentActiveRelay):
      return currentActiveRelay
    return 0

function state Machine Tick():
  evaluate Phase Health()

  case STATE_EVALUATE:
    desired = choose Target Relay()
    if desired != currentActiveRelay
      or activePhaseHasFault(currentActiveRelay):
      turn All Relays Off()
      currentActiveRelay = 0
      stateTimer = millis()
      state = STATE_DEADTIME

  case STATE_DEADTIME:
    if millis() - stateTimer >= CONTACTOR_DEAD_TIME_MS:
      target Relay = choose Target Relay()
      state = STATE_ENGAGE

  case STATE_ENGAGE:
```

```
      if targetRelay in {1,2,3} and phaseAcceptableGeneral(targetRelay):
        energizeRelay(targetRelay)
        recordSwitchForLockoutWindow()
      else:
        energizeRelay(0)
      state = STATE_EVALUATE

    if switchCountInWindow > SWITCH_LOCKOUT_THRESHOLD within
SWITCH_LOCKOUT_WINDOW_MS:
      turnAllRelaysOff()
      lockoutReason = "RAPID SWITCHING"
      state = STATE_LOCKOUT

    if loadCurrent >= OVERCURRENT_TRIP_A sustained for OVERCURRENT_TRIP_HOLD_MS:
      turnAllRelaysOff()
      lockoutReason = "OVERCURRENT"
      state = STATE_LOCKOUT

    case STATE_LOCKOUT:
      hold()
```

Algorithm 3: Display Update Routine

```
function updateDisplay():
    if now() - lastPageChange >= DISPLAY_GLIDE_MS:
      currentPage = (currentPage % 4) + 1
      lastPageChange = now()
      pageNeedsRedraw = TRUE

    if pageNeedsRedraw:
      clearScreen()
      drawStaticFrame(currentPage)
      pageNeedsRedraw = FALSE
    else:
      updateDynamicFields(currentPage)

    every 1000ms:
      pushVoltageSampleToGraphBuffer(activePhaseVoltage)
```

Algorithm 4: Load-Side Protection Logic

```
function checkLoadProtection():
    if loadCurrent >= OVERCURRENT_WARNING_A:
      raiseWarningFlag("Load Current >80A - Warning")

    if loadCurrent >= OVERCURRENT_TRIP_A:
      if overcurrentStartTime == 0:
        overcurrentStartTime = now()
      if now() - overcurrentStartTime >= OVERCURRENT_TRIP_HOLD_MS:
        turnAllRelaysOff()
        lockoutReason = "OVERCURRENT"
        state = STATE_LOCKOUT
    else:
      overcurrentStartTime = 0

    if abs(currentPF - referencePF) > PF_CHANGE_THRESHOLD:
      if pfChangeStartTime == 0:
        pfChangeStartTime = now()
      if now() - pfChangeStartTime >= PF_CHANGE_HOLD_MS:
        raiseWarningFlag("Power Factor Change Detected")
    else:
      pfChangeStartTime = 0
      referencePF = currentPF
```

2.3.2 Sensor Acquisition

Four PZEM-004T modules share a single transmit line, each with its own receive pin. Before each read, the firmware re-initializes the universal asynchronous receiver–transmitter (UART) on the correct receive pin and discards stray bytes. All modules share the same Modbus address, safe because exactly one is electrically selected at any moment. The sampling interval is 1 Hz.

2.3.3 Switching State Machine

The switching decision is separate from the act of switching. In automatic mode, phases are checked in priority order (1, 2, 3), and the first phase that is valid, fully stable for the required one-hour recovery window (per Algorithm 2), free of consecutive faults, and freshly sampled is selected. If no phase qualifies, hysteresis keeps the current phase unless it has tripped. The state machine enforces break-before-make sequencing through three states: EVALUATE, DEADTIME (1000 ms with all relays open), and ENGAGE (final stability check before closing). Voltage is independently verified at three points before mains is connected to the load. Figure 5 shows the state diagram.

Recent research on contactor-based ATS systems has demonstrated the importance of controlled switching sequences, with optimized relay sequencing achieving transfer times as low as 14.1 ms (Buică et al., 2026). The proposed system's three-state structure provides similar predictability.

2.3.4 Load-Side Protection

If load current reaches or exceeds 80 A, a display-only warning is raised. If it stays at or above 95 A for 5 seconds, the system enters LOCKOUT, opening all relays. The 5-second hold was verified thermally safe using the adiabatic limit in Equation 6:

$$I^2t \leq k^2S^2 \qquad (6)$$

For k = 115 and S = 16 mm², the limit is 3,385,600 A²s. The trip's let-through energy is given by Equation 7:

$$I^2t = 95^2 \times 5 = 45{,}125A^2s \qquad (7)$$

This is approximately 75 times below the adiabatic limit, confirming thermal safety. Evaluated at the highest injected value of 98 A ($98^2 \times 5 = 48{,}020$ A²s), the margin is still about 70 times.

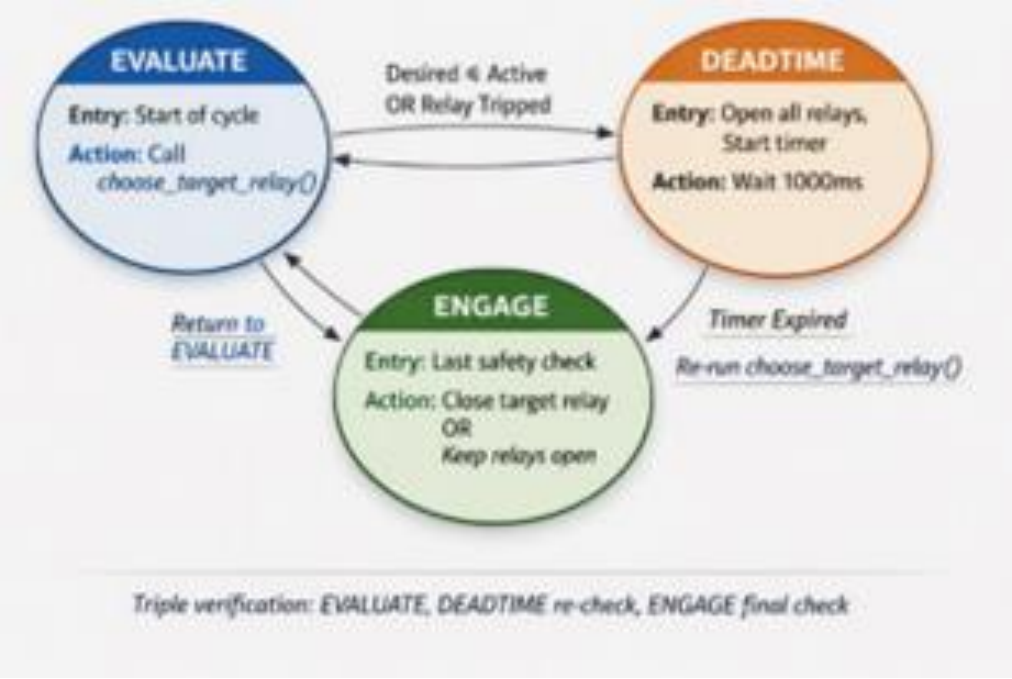


Figure 5: Phase Selection State Diagram

2.4 Component Sizing

2.4.1 Load Estimation

Table 4 outlines a representative connected load profile for a middle-income apartment in Benin City. The total connected load for the target residential profile is evaluated at 12,185 W. To establish the maximum continuous design current (I_B) before applying diversity factors, the assumed nominal utility supply voltage (V) is defined as 230 V, and the average power factor (cos θ) is estimated at 0.85 to account for the inductive nature of the connected load (comprising air conditioners, refrigerators, and water pumps).

Table 4: Estimated Maximum Connected Load for a Typical Residential Apartment in Benin City

APPLIANCE CATEGORY	EQUIPMENT	RATED POWER (W)	QUANTITY	TOTAL POWER (W)
Lighting	LED bulbs	15	15	225
Ventilation	Ceiling fans	90	4	360
Entertainment	LED TVs	150	2	300
Refrigeration	Refrigerator	300	1	300
Refrigeration	Deep freezer	500	1	500
Air Conditioning	1 HP Split AC unit	1000	3	3000
Water Supply	1 HP Borehole pump	1500	1	1500
Laundry	Washing machine	800	1	800
Heating & Kitchen	Water heater	1500	2	3000
Heating & Kitchen	Microwave oven	1000	1	1000
Heating & Kitchen	Electric iron	1200	1	1200
Total				**12,185**

The base design current is calculated from Equations 8 and 9:

$$I_B = \frac{P_{total}}{V \times \cos\theta} \quad (8)$$

$$I_B = \frac{12185}{230 \times 0.85} = 62.33 \text{ A} \quad (9)$$

This calculation establishes the absolute worst-case steady-state current without applying a diversity factor.

2.4.2 Contactor and MCB Rating

The system utilizes S9511M7 contactors (220 V datasheet rating, operated here from the 230 V nominal supply) rated for the AC-3 utilization category. This AC-3 rating certifies the hardware for motor-starting and motor-breaking duties, ensuring suitability for the evaluated 62.33 A highly inductive residential load profile, which includes multiple 1 HP air conditioners, refrigeration compressors, and a borehole pump. A 1.5 safety multiplier applied to the design current (62.33 A) gives Equation 10:

$$I_{contactor} \geq I_B \times 1.5 = 62.33 \times 1.5 = 93.5 \text{ A} \quad (10)$$

A 100 A contactor is selected. A 63 A MCB protects against short-circuit faults without nuisance tripping.

2.4.3 Cable Sizing

The internal power wiring utilizes a 16 mm² single-core PVC-insulated copper cable. According to BS 7671 (BSI & IET, 2008; Reference Method B, for cables enclosed in conduit or trunking on a wall), the base current-carrying capacity of this conductor is 76 A at an ambient temperature of 30 °C. Because the conductors are housed within a closed electrical enclosure operating in Benin City's climate, a conservative ambient temperature of 40 °C is assumed, requiring a derating factor of 0.87 for 70 °C thermoplastic insulation. The effective current-carrying capacity (I_z) is therefore given by Equation 11:

$$I_z = 76 \text{ A} \times 0.87 = 66.12 \text{ A} \quad (11)$$

Because the interlocking design ensures that only one phase carries the load at any given time,

no grouping factor is applied. The selection of the 63 A MCB and the 16 mm² cable satisfies the fundamental overload coordination requirement ($I_B \leq I_n \leq I_z$), as shown in Equation 12:

$$62.33\ \text{A} \leq 63\ \text{A} \leq 66.12\ \text{A} \qquad (12)$$

To ensure thermal safety under fault conditions, the selected MCB features a rated short-circuit breaking capacity (I_{cn}) of 6000 A, providing a wide withstand margin against the maximum prospective short-circuit fault levels typical of a single-phase residential service connection. Furthermore, for the short internal conductor run of approximately 0.6 m, the steady-state voltage drop is calculated using the tabulated parameter of 2.8 mV/A/m and, conservatively, the 63 A MCB rating as the current (Equation 13); the corresponding percentage drop is given by Equation 14:

$$\Delta V = \frac{2.8 \times 63 \times 0.6}{1000} = 0.106\ \text{V} \qquad (13)$$

$$\%\ \text{Voltage Drop} = \frac{0.106}{230} \times 100\% = 0.046\% \qquad (14)$$

This minimal voltage drop verifies that the 16 mm² cable satisfies all current-carrying capacity, local thermal derating, overload-coordination, and voltage-drop requirements without relying solely on the conductor's nominal ampacity.

2.4.4 Battery Backup

The target backup runtime is approximately 5 hours during a supply outage. The control unit's continuous load is the ESP32, four PZEM-004T modules, level shifters, and TFT display. Taking a combined continuous draw on the order of 400–500 mA at 5 V (Table 3 lists about 400 mA before the relay and switching draw), and using 450 mA, the required capacity is given by Equation 15:

$$\text{Required capacity} = 450\ \text{mA} \times 5\ \text{h} = 2{,}250\ \text{mAh} \qquad (15)$$

A two-cell 18650 pack configured in parallel, using cells rated at 2,000 mAh each, gives a combined capacity of 4,000 mAh. In energy terms, the requirement is 2,250 mAh × 5 V ≈ 11.25 Wh; the pack provides 4,000 mAh × 3.7 V = 14.8 Wh nominal. At 85–90% boost-converter efficiency, about 12.6–13.3 Wh is delivered to the 5 V rail, a margin of approximately 12–18% over the 11.25 Wh requirement. This assumes the full nominal capacity is usable; if only about 80% of it is usable, the delivered energy falls to about 10.1–10.7 Wh, which would support roughly 4.5–4.7 h rather than 5 h. The converter efficiency and the usable capacity were not measured, so these figures are estimates.

2.5 Testing Procedures

Testing used a simulated three-phase setup with variable autotransformers and a resistive load bank. The bench could not supply 80–98 A, so load-side protection was verified by injecting simulated current values into the firmware. Seven scenarios were tested: voltage/current sensing accuracy, switching response time, voltage stability evaluation, load-side protection, power-factor change detection, interlocking, and fail-safe operation. The testing methodology follows established practices in low-cost monitoring system validation (Cárdenas Magaña et al., 2026). The number of trials per condition, instrument make/model and calibration status, sampling interval, and pass/fail criteria are summarized in Table 5. Figures 6–8 show the completed prototype, the PZEM-004T modules with their MCBs, and the microcontroller unit.

3.0 Results and Discussion

3.1 Sensing Accuracy

Tables 6–8 present voltage sensing accuracy for the three phases, and Table 9 presents current sensing accuracy. All percentage errors have been recalculated using the formula: Error (%) = 100 × (PZEM reading − reference reading) / reference reading.

Table 5: Test Procedures and Conditions

Test Scenario	Description	Instruments	Trials	Pass/Fail Criteria
Voltage/Current Sensing	Compare PZEM-004T vs. calibrated digital multimeter	Calibrated digital multimeter	5 voltage points/phase, 4 current points	Error ≤ ±2% voltage, ≤ ±0.5% current
Switching Response	Measure time from the first out-of-band sample received to load reconnection	Oscilloscope	3 phase-transfer events	≤ 5 s
Voltage Stability	Apply transient sags/spikes and verify timer behavior	Variable autotransformers	4 scenarios (2 s sag, hard-limit fault, timer reset, 1-hr recovery)	No switching for grace-zone excursions <5 s; immediate switching for hard-limit faults
Load-Side Protection	Inject simulated current values	Firmware injection	9 current levels	Warning at 80 A, trip at 95 A/5 s
Power Factor Change	Inject simulated PF shift from 0.90 to 0.70	Firmware injection	1 scenario	Warning after 5 s
Interlocking	Attempt overlapping phase connections	Auxiliary contacts, firmware logs	100 cycles	Zero overlaps
Fail-Safe	Power down/reboot MCU	Oscilloscope, multimeter	4 conditions (normal, power loss, reboot, emergency stop)	All contactors OFF



Figure 6: Completed Prototype Assembly



Figure 7: PZEMs with MCBs



Figure 8: Microcontroller Unit

Table 6: Voltage Sensing Accuracy – Red Phase

Test Point (V)	PZEM Reading (V)	Multimeter Reading (V)	Signed Error (%)	Absolute Error (%)
180	179.4	180.2	−0.44	0.44
200	199.3	199.8	−0.25	0.25
220	219.9	220.1	−0.09	0.09
240	239.9	240.3	−0.17	0.17
260	258.4	259.7	−0.50	0.50

Table 7: Voltage Sensing Accuracy – Yellow Phase

Test Point (V)	PZEM Reading (V)	Multimeter Reading (V)	Signed Error (%)	Absolute Error (%)
180	179.6	180.4	−0.44	0.44
200	200.4	199.7	+0.35	0.35
220	219.4	220.2	−0.36	0.36
240	240.5	239.8	+0.29	0.29
260	259.1	260.4	−0.50	0.50

Table 8: Voltage Sensing Accuracy – Blue Phase

Test Point (V)	PZEM Reading (V)	Multimeter Reading (V)	Signed Error (%)	Absolute Error (%)
180	180.3	179.8	+0.28	0.28
200	199.7	200.3	−0.30	0.30
220	220.6	219.9	+0.32	0.32
240	239.3	240.3	−0.42	0.42
260	260.6	259.9	+0.27	0.27

Table 9: Current Sensing Accuracy

Test Point (A)	PZEM Reading (A)	Multimeter Reading (A)	Signed Error (%)	Absolute Error (%)
2.0	2.01	2.02	−0.50	0.50
5.0	4.96	4.98	−0.40	0.40
8.0	8.02	8.03	−0.12	0.12
12.0	11.94	11.99	−0.42	0.42

The maximum absolute voltage error across all three phases was 0.50%. The maximum absolute current error was 0.50% (2 A test point; 0.495% before rounding, i.e., at the limit of the ±0.5% criterion). These results are within the ±2% voltage and ±0.5% current targets; current accuracy was verified only at the 2–12 A test points the bench could supply. The accuracy is at the PZEM-004T datasheet limit of ±0.5%, reflecting controlled bench conditions. These results are consistent with recent findings on the PZEM-004T's performance, where mean absolute errors of 0.31 V for voltage and 0.008 A for current were reported (Cárdenas Magaña et al., 2026). For comparison, an average error of ±1.8% has been reported for a three-phase monitoring prototype (Mustofa, 2026); the errors measured here are lower, although instruments and test conditions differ.

3.2 Switching Response Time

Table 10 summarizes switching response times. The mean transfer time is calculated from the three phase-transfer events only; the all-phases-disconnect event is reported separately and not included in the mean. The "Engagement Time" column represents the period after the dead time needed to energize the relay, close the contactor and reconnect the load. The target phase had already completed its 1-hour recovery window before the fault, so no stability wait is included. Detection time is measured from the first out-of-band sample received by the firmware; the wait for that sample can add up to about one 1 Hz sampling interval, so the end-to-end worst case is roughly 3 seconds, still within the 5-second target.

Table 10: Switching Response Time Results

Switching Event	Detection Time (s)*	Dead Time (s)	Engagement Time (s)	Total Switching Time (s)
Phase 1 → Phase 2	0.15	1.00	0.78	1.93
Phase 2 → Phase 3	0.16	1.00	0.82	1.98
Phase 1 → Phase 3	0.14	1.00	0.75	1.89
All Phases → Disconnect	0.12	1.00	N/A	1.12

* Measured from the first out-of-band sample received by the firmware; the wait for that sample (up to about 1 s at the 1 Hz update rate) is not included. Mean Phase-Transfer Time = (1.93 + 1.98 + 1.89) / 3 = 1.93 s

The measured transfer time was shorter than the 20 s reported by Akinola et al. (2024), although the test conditions and timing definitions should be compared before drawing a direct performance conclusion. Recent research on contactor-based ATS systems has demonstrated even faster transfer times of 14.1–15.7 ms using optimized AC coil contactors (Buică et al., 2026); however, those systems do not incorporate the time-based stability evaluation that distinguishes the proposed design.

The break-before-make sequence includes a 1 s dead time. The manuscript does not claim that this interval eliminates arcing or arc-flash risk. During phase transfers, the firmware enforces a 1000 ms dead time strictly as a break-before-make safety timing mechanism to prevent catastrophic phase-to-phase cross-conduction. This dead time does not eliminate the arcing or arc-flash risks inherent to breaking inductive load currents; instead, arc suppression is managed entirely by the contactor's mechanical design and internal arc chutes.

3.3 Voltage Stability Evaluation

A 2-second sag from 220 V (the bench setting used for this test, inside the acceptable band) to 175 V (grace zone) was flagged as transient but not treated as a fault, and the system did not switch. When voltage fell below 170 V (hard limit), an immediate fault was flagged, and the system switched to Phase 2. An out-of-band spike reset the 5-second timer to zero. The 1-hour recovery window was verified using an accelerated 30-second test build and extended real-time observation of the production firmware. Both timers share the same reset logic and behave consistently.

The four-band classification provides effective hysteresis, preventing relay chatter at threshold boundaries. The timers are related to IEEE Std 1159-2019 by duration only (Section 1.1.4): the 5-second grace period lies in the temporary category (>3 s, up to 1 minute), and the 1-hour window is far longer than the 1-minute lower limit of the long-duration category. They are the authors' own design choices, and no compliance with the standard is claimed.

3.4 Load-Side Protection

Table 11 presents the load-side protection response. This is a firmware/injection test; no current of 80–98 A flowed through the PZEM-004T, CT, contactors, or load-side wiring. Power factor change detection was verified: a deviation of 0.20 against the 0.15 threshold triggered a warning after the full 5-second hold period. The integration of load-side monitoring addresses a critical gap identified in the literature, where existing phase selectors monitor only grid-side parameters.

A future test plan using a suitably rated controlled current source or load bank able to supply at least 100 A at 230 V in adjustable steps is proposed. This test should be carried out under the supervision of a qualified electrical engineer, with correctly rated upstream protection and an emergency stop in place.

3.5 Interlocking System

Table 12 presents interlocking test results. The 100% result means no overlap was observed in 100 attempted cycles under the test conditions; it is not a guarantee of zero risk in all operating conditions.

Table 11: Load-Side Protection Response (Firmware Injection Test)

Injected (Simulated) Load Current (A)	System Response	Firmware/Relay Action
50–70	Normal	No action
80–93	Warning	Warning flag on TFT display
95	Trip after 5 s	Contactors commanded open by firmware; no physical current interrupted
98	Trip after 5 s	Contactors commanded open by firmware; no physical current interrupted

Table 12: Interlocking System Test Results

Test Scenario	Cycles Tested	Attempted Overlaps	Actual Overlaps	Interlock Response
Hardware Only	50	50	0	Correctly prevented
Firmware Only	25	25	0	Correctly prevented
Both	25	25	0	Correctly prevented
Total	**100**	**100**	**0**	**100% Success**

The hardware interlock prevented physical overlap, and the firmware's break-before-make sequencing prevented software overlap. Together they achieved 100% success in preventing overlapping phase connections across the 100 test cycles. This dual-layer approach addresses a critical safety concern in multi-contactor systems: preventing two phases from being connected to the same load simultaneously. Recent research on ATS failures has documented severe consequences of simultaneous connection, including short circuits and fire hazards (Buică et al., 2026).

3.6 Fail-Safe Operation

Table 13 presents fail-safe test results. The system defaults to OFF on MCU power loss, preventing a contactor from remaining closed without supervision. This fail-safe design is critical, as recent research has documented dangerous failure modes in commercial ATS devices lacking such protection, including uncontrolled actuator operation, overheating, and potential fire hazards (Buică et al., 2026).

3.7 Bill of Materials

Table 14 presents the bill of materials. The total listed materials cost is ₦242,100. The enclosure (₦43,000) and four PZEM-004T modules (₦54,800) account for 40.4% of this total (97,800 / 242,100 = 40.4%). This is significantly more affordable than imported automatic transfer switches, which can cost upwards of ₦500,000. Recent research on low-cost ATS solutions has demonstrated that while budget devices may appear cost-effective at point of purchase, their downstream failure costs can far exceed the initial saving (Buică et al., 2026).

3.8 Comparison with Existing Design

Table 15 compares the proposed system with existing designs, with appropriate citations to the source literature for each design category.

3.9 Validation of Objectives

Table 16 maps each objective to its test result.

Table 13: Fail-Safe Operation Test Results

Condition	Esp32 State	Relay Input	Contactor State	Response
Normal	Running	5 V (HIGH)	Energized	Active
Power Loss	Off/Floating	≈0.45 V (LOW)	De-energized	Safe
Reboot	Restarting	≈0.45 V (LOW)	De-energized	Safe
Emergency Stop	Any	N/A	De-energized	Safe

Table 14: Bill of Materials for the Constructed Prototype

Item	Description	Quantity	Unit Cost (₦)	Total (₦)
ESP32 DevKit V1	Microcontroller	1	6,900	6,900
PZEM-004T	Voltage/current sensor	4	13,700	54,800
S9511M7 Contactor	100 A, 3-pole (with inbuilt auxiliary contact)	3	15,000	45,000
CHNT NXB-63 MCB	63 A, 2-pole	3	8,000	24,000
RCCB	63 A, 30 mA, 2-pole	1	9,000	9,000
5 V Relay Module	1-channel	3	1,400	4,200
TFT Display	2.8-inch SPI	1	8,900	8,900
18650 Li-ion Battery	2000 mAh	2	2,000	4,000
Wiring and Accessories	Cables, connectors	1	17,000	17,000
Auxiliary Contact Block	Add-on NC block (61-62), one extra per contactor	3	2,000	6,000
AC-DC Power Supply	HLK-PM01	1	4,500	4,500
BSS138 Level Shifter	4-channel	1	1,500	1,500
Emergency Stop Button	Mushroom head, NC	1	2,500	2,500
Enclosure	400 × 300 × 180 mm	1	43,000	43,000
Expansion Board	—	1	5,000	5,000
Snubber resistor	100 Ω, 1 W	3	100	300
Snubber capacitor	0.1 µF, polypropylene	3	200	600
MOV	10D471	3	200	600
Pull-down resistor	1 kΩ, one per switching channel	3	100	300
Charger module (LX-2BUPS)	Li-ion charging	1	4,000	4,000
Total				242,100

Table 15: Performance Comparison with Existing Designs

Metric	Comparator-Based Designs	Threshold-Based Designs	Proposed System	Supporting Evidence
Voltage Evaluation	Instantaneous	Instantaneous	Time-based (5 s + 1 hr)	Comparator circuits (Asiwe & Usiaade, 2021; Oduobuk et al., 2014; Ezirim et al., 2015) and threshold logic (Singh et al., 2017; Mbaocha, 2012) react instantly; this work introduces deliberate delay.
Load Monitoring	Absent	Absent	Integrated (ESP32 + PZEM sensors)	Earlier designs focus only on voltage; this work adds real-time load sensing.
Switching Time	Not directly comparable	Not directly comparable	~1.93 s (avg)	Transfer times are not consistently reported for comparator/threshold designs. The one reported figure (20 s; Akinola et al., 2024) is longer than the 1.93 s measured here, but test conditions and timing definitions differ, so direct comparison requires identical test conditions.
Unnecessary Switching	Reported as frequent in literature	Reported as frequent in literature	Reduced by design (only sustained faults trigger transfers)	Literature notes nuisance transfers in instantaneous systems; dual-timescale algorithm reduces false switching.
Load Protection	None	Limited or absent	Yes (80 A warning, 95 A trip; verified by firmware injection)	Threshold-based designs provide at most limited protection; this work integrates full current monitoring and trip thresholds.
User Interface	None or LCD	LCD/Digital Display	TFT with trend visualization	Asiwe & Usiaade (2021) and Madueme et al. (2018) mention LCDs; this work advances to TFT with historical trends.
Fail-Safe Operation	Absent	Absent	Yes (1 kΩ pull-down)	Fail-safe defaults not reported in earlier works; this work introduces hardware pull-down for safety.

Table 16: Verification of Design Objectives

Objective	Target	Result	Status
Mechanical/Protection Unit	MCBs, RCCB, 100 A contactors	Installed as specified	✓ Achieved
Sensing System	ESP32, four PZEM-004T	±0.50% voltage, ±0.50% current (verified 2–12 A only)	✓ Achieved
Phase Selection Algorithm	5-second window, interlocking	100% interlock, <2 s switching	✓ Achieved
User Interface	TFT, pilot lights, override	All features tested	✓ Achieved
System Testing	<5 s, ±2%, 100 cycles	1.93 s, ±0.50%, 100 cycles; load-protection logic verified by current injection	✓ Achieved

3.10 Limitations

Several limitations of this study should be acknowledged:

1. High-current protection was verified by injected firmware values because the bench could not supply 80–98 A. No physical current in this range flowed through the PZEM-004T, CT, contactors, or load-side wiring. The results confirm the comparison logic, timing, and relay command only. Current sensing accuracy was physically verified only from 2 A to 12 A.
2. Sensor accuracy was verified at a limited number of test points (5 voltage points per phase, 4 current points), and no repeatability statistics or confidence intervals are provided.
3. The 1-hour recovery window was verified using an accelerated 30-second test build and extended real-time observation, not a full 1-hour test on every run.
4. Contactor endurance was not tested. The lifespan estimates are theoretical extrapolations from manufacturer data, not predictions of service life.
5. The system was tested on a controlled, simulated three-phase setup, not a live utility feeder.

4.0 Conclusion

This paper presented a microcontroller-based automatic phase selector using dual-timescale voltage stability evaluation. The system addresses the limitations of instantaneous-response designs by separating fault detection (5-second grace period) from long-term trust (1-hour recovery window), both operating over a four-band voltage classification.

Key findings:

1. Sensing accuracy: Maximum absolute voltage error of ±0.50% and maximum absolute current error of ±0.50%, within the ±2% and ±0.5% targets (current verified at 2–12 A only).
2. Switching response: Average phase-transfer time of 1.93 seconds, well within the 5-second target.
3. Voltage stability: The four-band algorithm successfully distinguished transient disturbances from sustained failures, with reset-on-bad-sample behavior at both timescales.
4. Load-side protection: Warning at an injected 80 A and commanded disconnection at an injected 95 A, verified by firmware injection only; the 5-second hold was verified thermally safe (~75x margin against the adiabatic limit).
5. Interlocking and fail-safe: No overlapping phase connection was observed in 100 test cycles; all contactors default to OFF on MCU power loss via the 1 kΩ pull-down resistor.
6. Cost-effectiveness: Total materials cost of ₦242,100, significantly below imported automatic transfer switches.

The dual-timescale approach should reduce unnecessary switching and contact wear, but this has not been quantified over a defined duration and requires further validation. The prototype demonstrates the feasibility of time-based phase selection. Future work should focus on physical high-current testing with a suitably rated load bank, extended endurance testing, remote monitoring and cloud integration (Mustofa, 2026), integration with alternative power sources (Sukadana et al., 2026), and machine learning for predictive maintenance (Khaldi et al., 2025).

Conflict-of-Interest Disclosure

The authors declare that they have no competing interests related to this manuscript.

Acknowledgements

The authors thank the staff of the Electrical Laboratory, University of Benin, for permitting

the use of the laboratory equipment and for their guidance during testing. This work was not funded.

References

Adamu, A. U. D., Mohammed, H., & Moshud, K. M. (2025). Construction of automatic phase selector for the generation of a steady power supply. *International Journal of Development Mathematics*, 2(3), 176–187. https://doi.org/10.62054-/ijdm/0203.12

Adeniyi, O. (2022). The economics of generator dependence among Nigerian SMEs. *Journal of Energy Policy Studies*, 14(2), 45–62.

Adesina, L. M., Ogunbiyi, O., & Jimada-Ojualope, B. (2024). Development of an automatic phase selector for Nigerian power utility customers. *ABUAD Journal of Engineering Research and Development*, 7(2), 16–26. https://doi.org/10.53982/ajerd.2024.0702.02-j

Akinola, O. A., Afolabi, A. S., Adebayo, A. T., Ojo, E. K., & Raji, A. A. (2024). Three phase microcontroller based automatic change-over selection switch. *LAUTECH Journal of Engineering and Technology*, 18(2), 161–174.

Akpan, E. P., Orike, S., & Odeyemi, F. M. (2019). An improved microcontroller-based automatic three-phase analyzer and selector. *Journal of Newviews in Engineering and Technology*, 1(1), 53–61.

Akinola, O. A., Afolabi, A. S., Adebayo, A. T., Ojo, E. K., & Raji, A. A. (2024). Three phase microcontroller based automatic change-over selection switch. *LAUTECH Journal of Engineering and Technology*, 18(2), 161–174.

Asiwe, U. M., & Usiaade, R. E. (2021). Design and construction of automatic phase selector using OP-AMP comparator. *Innovative Journal of Engineering Technology*, 2(1), 1–11. Retrieved from http://journals.rasetass.org/index.php/ijet/article/view/75

British Standards Institution (BSI), & Institution of Engineering and Technology (IET). (2008). BS 7671:2008 Requirements for electrical installations: IET wiring regulations (17th ed.). London, UK: BSI and IET.

Buică, E.-V., Militaru, A., Leț, D. D., & Andrei, H. L. (2026). Neutral conductor loss in residential photovoltaic installations: Overvoltage analysis and design of a contactor-based automatic transfer switch. *Energies*, 19(10), Article 2346. https://doi.org/10.3390/en19102346

Cárdenas Magaña, J. A., Mojica Magaña, A., & Hernández López, F. M. (2026). Experimental validation of a low-cost IoT-based residential electrical monitoring system using ESP32 and PZEM-004T. *International Journal of Electrical and Computer Engineering Research*, 6(2), 7–14. https://doi.org/10.53375/ijecer.2026.527

Espressif Systems. (2022). *ESP32-WROOM-32 datasheet*. Shanghai, China: Espressif Systems. Retrieved from https://www.-espressif.com/sites/default/files/documentation/esp32-wroom-32_datasheet_en.pdf

Ezirim, U. I., Oweziem, U. B., Obinwa, C. C., & Ekwueme, S. O. (2015). Design of an automatic power phase selector. *International Journal of Engineering and Innovative Technology (IJEIT)*, 5(2), 1–5.

Hidayat, K. M. W., & Al-Faris, M. G. (2025). IoT-based electrical power consumption

monitoring system in households using ESP32 and PZEM-004T. *Brilliance: Research of Artificial Intelligence*, 5(2), 1077–1081. https://doi.org/10.47709/-brilliance.v5i2.6368

IEEE. (2019). *IEEE recommended practice for monitoring electric power quality* (IEEE Std 1159-2019). IEEE. https://doi.org/-10.1109/IEEESTD.2019.8796486

Ish, U. (2024). Design and construction of an automatic phase selector for 3-phase power supply. *International Journal of Innovative Scientific and Engineering Technologies Research*, 12(3), 64–70.

Khaldi, B. F., Dekhandji, F. Z., & Recioui, A. (2025). Low-cost IoT-based smart meter for real-time power quality monitoring and disturbance detection using embedded 1D CNN. *Journal of Energy Systems*, 9(4), 365–379.

Madueme, V. C., Okoli, C. C., & Obiora, G. (2018). Design and construction of an automatic phase selector with digital display. *NEEE Journal of Research and Innovative Technology*, 1(1), 86–93.

Mbaocha, C. (2012). Smart phase change-over system with AT89C52 microcontroller. *IOSR Journal of Electrical and Electronics Engineering*, 1(3), 31–34.

Mustofa, A. B. (2026). Prototype of a three-phase voltage monitoring system for induction motor protection based on Arduino ESP32 with Telegram notifications. *International Journal of Health, Engineering and Technology*, 5(2), 1600–1606.

Odior, A. O., & Omadudu, C. M. (2013). Some factors responsible for erratic power supply in Benin City. *International Journal of System Assurance Engineering and Management*, 4(1), 48–56.

Oduobuk, E., Ettah, E., & Ekpenyong, E. (2014). Design and implementation of automatic three phase changer using LM324 quad integrated circuit. *International Journal of Engineering and Technology Research*, 2(4), 1–15.

Ofualagba, G., & Udoha, E. E. (2017). Design and simulation of automatic phase selector and changeover switch for 3-phase supply. *International Journal of Novel Research in Electrical and Mechanical Engineering*, 4(2), 28–35. Retrieved from http://www.noveltyjournals.com/viewpaper/Design-and-Simulation-of-Automatic-Phase-Selector

Sahara Reporters. (2023, October 15). Benin residents lament less than one hour of electricity daily. *Sahara Reporters*.

Singh, N., Kumar, N., & Kumar, A. (2017). Automatic active phase selector for single phase load from three phase supply. *International Journal and Magazine of Engineering, Technology, Management and Research*, 4(3), 460–463.

Sukadana, I. W., Prayoga, D., & Suriana, I. W. (2026). Contactor-based ATS-AMF system design and simulation for power continuity. *Journal of Electrical Engineering and Technology*, 21(1), 1–12.

Uchechukwu, O. (2015). Phase selection mechanism in power distribution systems. *Journal of Electrical and Electronic Engineering*, 10(2), 45–51.

Vanguard. (2023, December 10). BEDC announces eight-day blackout in Warri and Effurun. *Vanguard*.